Supplementary Experimental Procedures

Plasmid Construction

pCS9 was created by co-transforming linearized pRS315 and pRS416 respectively with a PCR fragment encoding *MVB12* or *VPS37* amplified from yeast genomic DNA, followed by plasmid rescue. Plasmids for the expression of GFP-tagged Ste3, Sna3 and ALP have been described: pJLU34 (Urbanowski and Piper, 2001); pGFP-Sna3 (Reggiori and Pelham, 2001); pRS426-GFP-ALP (Cowles et al., 1997). Plasmids encoding *VPS27* and *VPS23*, pRCP4 and pKEB73 respectively, have also been previously described (Bowers et al., 2004; Piper et al., 1995). pCS17 was created by tagging *VPS23* in pKEB73 using pFA6a-3HA-kanMX6 as previously described (Longtine et al 1998). pMVB12-YFP was constructed by PCR amplification of *MVB12* promoter and coding sequences from genomic DNA and co-transformation with a linearized vector containing the YFP coding region (Sheff and Thorn, 2004), followed by plasmid rescue. A two-step PCR procedure was used to add a single copy of the c-myc epitope flanked by *Bam*HI sites to the C terminus of *VPS37* in pCS27. Two PCR products, with homology to each other and together containing the entire sequence for the *Bam*HI flanked c-myc epitope, were amplified from yeast genomic DNA and co-transformed into linearized pRS416, followed by plasmid rescue. This introduced the sequence DPEQKLISEEDLLDP immediately before the stop codon of the ORF. Site-directed mutagenesis of pCS9, pCS25, pMVB12-YFP, pCS17 and pCS27 was accomplished using the QuikChange kit (Stratagene), and all mutations were verified by DNA sequencing of the entire gene.

Strain Construction

Yeast gene knockout collections in strain backgrounds BY4741, BY4742 and BY4743 were obtained from Open Biosystems (Huntsville, AL). Other strains used in this study are listed in Table S4.

To create Mvb12-GFP and Vps23-GFP-expressing strains, a C-terminal GFP tag was introduced at the endogenous *MVB12* or *VPS23* locus using pFA6a-GFP(S65T)-HIS3MX6 as described (Longtine et al., 1998). A two-step PCR procedure was used to

make SHY34 and CSY41. First, the KanMX module in strain SHY9 was replaced with NatMX using EcoRI-digested p4339 (Tong et al., 2001). A 2Kb fragment encoding the *vps4*Δ*::NatR* was then amplified from genomic DNA and used to disrupt *VPS4* in SHY13 and CSY49. *VPS23* was tagged with six copies of HA in strains listed in Table S4 using pYM17 as previously described (Janke et al., 2004). Epitope tagging of *VPS37* at the endogenous locus was accomplished using pFA6a-13myc-HIS3MX6 as described (Longtine et al., 1998).

Primer sequences used in plasmid and strain construction are available on request. Yeast gene knockout collections in strain backgrounds BY4741, BY4742 and BY4743 were obtained from Open Biosystems (Huntsville, AL). Other strains used in this study are listed in Table S4.

Protein Expression and Purification

DNAs coding for the appropriate regions of yeast Mvb12, Vps23, Vps28, and Vps37 (Fig. 2A) were amplified by PCR to generate cassettes containing the Shine-Delgarno translational start signal (Hierro et al., 2005) and cloned directly into the polycistronic pST39 vector (Tan, 2001). Both the full length and crystallized constructs contain the mutations Vps28^{C101A} and Vps37^{C123A}, which were introduced to reduce oxidation and non-specific aggregation. Constructs of the ESCRT-I complex were expressed in *Escherichia coli* BL21 RIL grown in TB medium (Sigma) and induced with 0.5 mM isopropylthiogalactoside (IPTG) at an OD_{600} = 1.0. Cultures were grown at 20^{o}C for 24 h after induction. Cells were lysed by sonication in 50 mM Tris pH 7.4, 300 mM NaCl, 3 mM β-mercaptoethanol (βME) supplemented with 100 µl of protease inhibitor cocktail (Sigma) per liter culture medium. ESCRT-I was isolated from the lysate using Talon-Co^{2+} resin (Clontech). The hexahistidine tag on Vps23 was removed with TEV protease in conjunction with dialysis against 50 mM Tris pH 7.4, 300 mM NaCl, 5 mM imidazole. Histidine-tagged TEV protease was removed from the protein sample by a second pass over a Talon-Co^{2+} affinity column. The purified protein complex was concentrated and run on a HiLoad 16/60 Superdex 200 column (Pharmacia) using 50 mM Tris pH 7.4, 150 mM NaCl, 5 mM DTT.

DNA coding for "mini-Vps27" was constructed by sequentially inserting artificial DNA sequences coding for residues 326-333, 445-450, and 522-527 of Vps27 in frame following DNA amplified from the yeast genome coding for Vps27 residues 169-323 in the context of the plasmid pGST2 (Sheffield et al., 1999). Artificial DNA sequences were optimized for expression in *E. coli* using DNAWorks version 3.1 (Hoover and Lubkowski, 2002). The resulting mini-Vps27 includes the FYVE domain, two UIMs and two P(S/T)XP motifs. The mini-Vps27 was expressed as a GST-fusion protein in *E. coli* BL21(DE3)Star (Invitrogen). The mini-Vps27 was purified using a similar lysis protocol as described for the ESCRT-I constructs. Purification was carried out using glutathione-Sepharose resin (GE Healthcare) in place of Talon-Co^{2+} resin. The final buffer for the purified protein was 10 mM Hepes pH 7.4, 150 mM NaCl.

DNA coding for Ub-Cps1(8-17)C was constructed as follows. DNA coding for residues 8-40 of *S. cerevisiae* carboxypeptidase S (Cps1) was amplified by PCR with two overlapping primers. The DNA for Cps1(8-40) was fused to the 3' end of the DNA for *S. cerevisiae* ubiquitin by PCR using overlapping primers. The resulting insert was cloned into vector pHIS2 (Sheffield et al., 1999) . The region covering ubiquitin and Cps1 (8-18) was amplified by PCR from pHIS2-Ub-Cps1 (8-40) and cloned into the vector pGST2 (Sheffield et al., 1999) . Site-directed mutagenesis was used to replace the C-terminal residue of this fragment (18) with a cysteine to facilitate chemical conjugation. The resulting pGST2-Ub-Cps1(8-17)C was transformed to *E. coli* BL21(DE3) and purified by the method described for pGST2-mini-Vps27. The purified protein was flash frozen upon the conclusion of purification and stored at -80 ^{o}C until used.

Crystallization and Data Collection

In order to crystallize the ESCRT-I core complex, the Vps23 UEV domain and the Vps28 C-terminal domain were deleted. The N-terminal 21 residues of Vps37, previously shown to contribute to aggregation (Teo et al., 2006), were deleted. Residues 82-101 of Mvb12 were dispensable for complex formation, and were therefore deleted. Functional analysis of the Vps37 Δ1-21 and Mvb12 Δ82-101 constructs revealed that neither region is required for cargo sorting (Table S3). Crystals of the Vps23 Δ1-214: Vps28 Δ119-242: Vps37 Δ1-21: Mvb12 Δ82-101 complex were obtained by streak seeding upon mixing of

the drop to crystals that diffracted anisotropically to a maximum resolution of 2.7 Å in two directions and 3.3 Å in a third. Crystals appeared overnight and were harvested for data collection after two or more days. The crystals were cryoprotected in mother liquor supplemented with 25% glycerol and flash frozen in liquid nitrogen. Selenomethionyl crystals were prepared under identical conditions as the native crystals. Heavy atom derivatives were prepared by soaking native crystals for 15 to 30 minutes in mother liquor supplemented with 1 mM $AuCl_3$ or K_2PtCl_4. Diffraction data were collected at Advanced Photon Source beamlines SER-CAT 22-ID and 22-BM and processed using HKL2000 (HKL Research).

Structure Determination

Heavy atom sites were located and refined in SOLVE (Terwilliger and Berendzen, 1999). Six Se, 2 Au, and 1 Pt site were located, and the density map was improved using density modification in RESOLVE (Terwilliger, 2000). The map was traced using the model building program O (Jones et al., 1991) after manually placing the previously determined structure of the ESCRT-I core complex, PDB-ID 2F66. Cycles of manual building and refinement were carried out to improve the model. Refinement was carried out in CNS (Brunger et al., 1998) and included least-squares minimization, simulated annealing and individual temperature factor refinement.

Sedimentation Equilibrium

Sedimentation equilibrium experiments were conducted at 4.0°C on a Beckman Optima XL-A analytical ultracentrifuge. Samples were purified by gel filtration in 50 mM Tris pH 7.4, 150 mM NaCl, 5 mM βME, and loaded at three different concentrations corresponding to loading A280 of approximately 0.4, 0.8 and 1.2. Each loading concentration, when analyzed independently, returns an identical molecular mass within the error of the method. Data were acquired at 6, 8, 10 and 12 krpm as an average of 4 absorbance measurements at a wavelength of 280 nm and a radial spacing of 0.001 cm. Equilibrium was achieved within 48 hours. No evidence for higher mass species or samples losses was noted. Data were analyzed in SEDPHAT 4.3 in terms of a single ideal solute (Schuck, 2003)

(http://www.analyticalultracentrifugation.com/sedphat/sedphat.htm). Solution densities were determined experimentally at 20° C on a Mettler-Toledo DE51 density meter and corrected to values for ρ at 4.0°C. Protein partial specific volumes (ν) calculated in SEDNTERP (Philo, J. ; http://www.jphilo.mailway.com/) based on the amino acid sequence. Excellent data fits were observed.

Sedimentation Velocity

Sedimentation equilibrium experiments were conducted at 4.0°C on a Beckman Optima XL-A analytical ultracentrifuge. Samples (loading volume of 350 µl) were studied at a loading A_{280} of 1.00 at 50 and/or 58 krpm. Data were acquired as single absorbance measurement at 280 nm and a radial spacing of 0.003 cm with 120-150 scans collected at 2.2 minute intervals. Data were analyzed in SEDFIT 9.4 in terms of a single solute or a c(s) distribution (Lebowitz et al., 2002) (http://www.analyticalultracentrifugation.com/default.htm). Sedimentation coefficients s were corrected to $s_{20,w}$ based on the solvent density and viscosity (η) calculated based on the composition in SEDNTERP (Philo, J. ; http://www.jphilo.mailway.com/). Data obtained from full-length heterotetrameric ESCRT-I were analyzed in terms of a single discrete species, returning a corrected sedimentation coefficient $s_{20,w}$ of 4.15 ± 0.05 S (Fig. 2E). This species is elongated with a frictional ratio of 1.9. The crystallized Vps23 Δ1-214: Vps28 Δ119-242: Vps37 Δ1-21: Mvb12 Δ82-101 contains a major species that represents 90% of the loading absorbance and is presumed to represent the monomeric heterotetramer. This species has an experimental sedimentation coefficient of 3.25 ± 0.05 S. The experimentally determined value of the sedimentation coefficient corresponds to a frictional ratio of 1.8. Structural data were used to calculate the sedimentation coefficient based on a shell model using the program HYDROPRO (Garcia de la Torre et al., 2000), (http://leonardo.fcu.um.es/macromol/programs/hydropro/hydropro.htm).

Modeling of Hydrodynamic Data

The crystallographic coordinates of the ESCRT-I heterotetramer yielded a computed Stokes radius R_H = 4.48 nm, compared to the experimental value of 4.76 nm as determined by analytical ultracentrifugation (AUC). In the crystal Vps37 residues 23-41

are held in place by lattice contacts only, and have no direct contact with the rest of the structure. Vps37 residues 42-46 are completely absent from density, and furthermore residues in the loop from 47-61 have very high B-factors. To address the apparent mobility of the N-terminus of Vps37 in modeling the solution structure of the crystallized construct, residue 61 was chosen as a pivot point and residues 23-60 were repositioned until the calculated R_H agreed within 0.04 nm. The Vps23 Δ1-200 construct has an experimental R_H = 5.36 nm determined by AUC. The structure of Vps23 Δ1-200 was derived from the solution structure of the crystallized construct after extending the helical residues 23-31 of Vps37 to include the missing residues 1-21 in a helical conformation, as predicted by secondary structure analysis (Rost and Liu, 2003). Mvb12 residues 82-101 were modeled in an arbitrary loop conformation, again following secondary structure prediction analysis. The coordinates of the C-terminal domain of Vps28 omitted from the crystallized structure were obtained from PDB entry 2G3K (Pineda-Molina et al., 2006). Once an approximate solution was obtained, the linker between the core N-terminal domain of Vps28 and C-terminal domain of Vps28 was constructed in an arbitrary loop conformation consistent with secondary structure prediction. The position of this domain was adjusted until the calculated R_H agreed with the experimental value to within 0.04 nm. The solution structure of intact ESCRT-I was derived using the solution structure of the Vps23 Δ1-200 as a starting point. The structure of the Vps23 UEV domain was obtained from PDB entry 1UZX (Teo et al., 2004). Polyproline tracts were modeled in a polyproline type II (PPII) conformation, and the remainder of the linker was modeled in an arbitrary loop conformation consistent with secondary structure prediction. The position of the UEV domain was modified until the calculated R_H agreed with experiment to within 0.02 nm. The final model was subjected to 200 cycles of conjugate gradients energy minimization with CNS (Brunger et al., 1998). In the final model, the linker between the core portion of Vps28 and the start of the Vps28 C-terminal domain spans 30 residues and 38 Å. The Vps23 core-UEV linker spans 60 residues and 44 Å. The C-terminus of Mvb12 contains 20 residues and extends 29 Å. On the basis of polymer theory, the linkers are predicted to extend $l_p \bullet \sqrt{2 \bullet n}$ (Yamakawa, 1971), where l_p = 4 Å is the persistence length of a denatured and disordered polypeptide modeled as a wormlike chain (Buscaglia et al., 2006). This equation predicts that the Vps28 and Vps23

linkers, and the Mvb12 C-terminal extension should extend 31, 44, and 25 Å respectively, in close agreement with the model.

Supplementary Figure Legends

Figure S1. Role of Vps36 in Mvb12 Recruitment and Effect of Stalk Mutants on CPY Sorting and ESCRT-I Stability

(A) Mvb12 recruitment does not require *vps36*Δ. The chromosomal copy of *MVB12* was tagged with GFP in wild type and *vps36*Δ cells and visualized in live cells. (B) CPY sorting defects in stalk mutants of Vps23, Mvb12 and Vps37. CPY was detected by colony overlay assay from *mvb12*Δ, *vps23*Δ *or vps37*Δ strains containing plasmids for the expression of the indicated mutant or wild type forms of Mvb12, Vps23 or Vps37. (C) Effect of stalk mutants on the stability of ESCRT-I subunits. Plasmids for the expression of wild type or mutant forms of Vps23-3HA, Mvb12-YFP or Vps37-myc were transformed into *vps23*Δ, *mvb12*Δ or *vps37*Δ strains that additionally contained integrated tagged copies of Vps37-13myc, Mvb12-GFP and/or Vps23-6HA as indicated. Cell lysates were subjected to SDS-PAGE, and steady-state levels of each subunit were detected by western blotting with antibodies to myc, HA or GFP. Dpm1 served as a loading control.

Figure S2. Size Exclusion Chromatography of ESCRT Complexes.

(A) Analysis of recombinant ESCRT-I, II, and I-II complexes on a Superdex 200 16mm x 300 mm column monitored by absorption at 280 nm. (B) Best fit of ESCRT complex apparent molecular weights to standards. The apparent molecular weights are sensitive to small errors in elution volume (an error of 0.1 ml at an elution volume of 11 ml corresponds to 15 kDa error in molecular weight), and vary slightly with the column used. Sizing on a 16 mm x 600 mm column, the same size used by Emr and colleagues (Chu et al., 2006) and Babst and colleagues (Curtiss et al., 2006), yields a molecular weight of 340 kDa for recombinant ESCRT-I, identical to the results obtained by these workers. Sizing on a 16mm x 300 mm column identical to that used by Williams and co-workers (Gill et al., 2007) leads to apparent molecular weights of 270, 205, and 440 kDa for recombinant ESCRT I, II, and I-II, respectively. (C) Size exclusion data are more appropriately modeled as a function of size, as opposed to mass (Cantor and Schimmel, 1980). Comparison of the intact ESCRT-I Stokes radius R_H derived from analytical

ultracentrifugation to the best-fit standard curve. The experimental $R_H = 6.10$ obtained from analytical ultracentrifugation for recombinant ESCRT-I corresponds precisely to the value expected from fitting to gel filtration standards. The standards (BioRad, Hercules, CA) consist of bovine thyroglobulin (670 kDa, $R_H = 8.5$ nm), bovine γ-globulin (158 kDa, $R_H = 5.3$ nm), chicken ovalbumin (44 kDa, $R_H = 2.7$ nm), and horse myoglobin (17 kDa, $R_H = 2.1$ nm).

Figure S3. Structure-Based Sequence Alignment of Vps23 and Vps28 Orthologs
Amino acid sequences of homologs of Vps23 and Vps28 were aligned using ClustalX (Thompson et al., 1997). Conserved residues are highlighted in dark blue, light blue and grey according to the respective degree of conservation from highest to lowest. Boxes indicated residues mutated in the study as shown in Table S3. Highlighted boxes show residues whose mutations were characterized in full as described in the text.

Figure S4. Structure-Based Sequence Alignment of Vps37 Orthologs and Secondary Structures of Mvb12
Amino acid sequences of homologs of Vps37 were aligned using ClustalX. Conserved residues are highlighted in dark blue, light blue and grey according to the respective degree of conservation from highest to lowest. The amino acid sequence of Mvb12 is not aligned but its sequence and secondary structure is shown. Boxes indicated residues mutated in the study as shown in Table S3. Highlighted boxes show residues whose mutations were characterized in full as described in the text.

Figure S5. The $Vps23^{M254D/L286D}$ **stalk mutant disrupts ESCRT-I assembly**
(A) Mvb12 localization depends on the integrity of the stalk. The wild type or M254D/L286D mutant form of Vps23 was expressed from a plasmid in *vps23*Δ *vps4*Δ strains containing chromosomally integrated Mvb12-GFP. (B) Ste3 and Sna3 sorting defects in $Vps23^{M254D/L286D}$ mutants. Wild type or mutant forms of Vps23 were expressed from plasmids in *vps23*Δ strains that also contained plasmids for the expression of either Ste3-GFP or Sna3-GFP, as indicated. (C) CPY sorting defects in the $Vps23^{M254D/L286D}$ stalk mutants. CPY was detected by colony overlay assay from *vps23*Δ strains containing

plasmids for the expression of the mutant or wild type forms of Vps23. (D, E) Vps23 M254D/L286D mutations have differential effects on Vps37 and Mvb12 binding. Detergent extracts prepared from *vps23*Δ mutants strains containing chromosomally expressed tagged forms of Vps37-13myc (D) or Mvb12-GFP (E) and plasmids for the expression of wild type or mutant forms of Vps23 were subjected to immunoprecipitation with anti-HA antiserum and Protein G-sepharose, resolved by SDS-PAGE, and analyzed by western blotting with mAbs to HA and either myc (D) or GFP (E). Bar = 2 μM.

References for Supplementary Experimental Procedures and Figure Legends

Bowers, K., Lottridge, J., Helliwell, S. B., Goldthwaite, L. M., Luzio, J. P., and Stevens, T. H. (2004). Protein-protein interactions of ESCRT complexes in the yeast Saccharomyces cerevisiae. Traffic *5*, 194-210.

Brunger, A. T., Adams, P. D., Clore, G. M., DeLano, W. L., Gros, P., Grosse-Kunstleve, R. W., Jiang, J. S., Kuszewski, J., Nilges, M., Pannu, N. S.*, et al.* (1998). Crystallography & NMR system: A new software suite for macromolecular structure determination. Acta Crystallogr. Sect. D-Biol. Crystallogr. *54*, 905-921.

Buscaglia, M., Lapidus, L. J., Eaton, W. A., and Hofrichter, J. (2006). Effects of denaturants on the dynamics of loop formation in polypeptides. Biophys. J. *91*, 276-288.

Cantor, C. R., and Schimmel, P. R. (1980). Biophysical Chemistry (San Francisco: W. H. Freeman).

Chu, T., Sun, J., Saksena, S., and Emr, S. D. (2006). New component of ESCRT-I regulates endosomal sorting complex assembly. J. Cell Biol. *175*, 815-823.

Cowles, C. R., Snyder, W. B., Burd, C. G., and Emr, S. D. (1997). Novel Golgi to vacuole delivery pathway in yeast: Identification of a sorting determinant and required transport component. Embo J. *16*, 2769-2782.

Curtiss, M., Jones, C., and Babst, M. (2006). Efficient cargo sorting by ESCRT-I and the subsequent release of ESCRT-I from multivesicular bodies requires the subunit Mvb12. Mol Biol Cell *18*, 636-645.

Garcia de la Torre, J., Huertas, M. L., and Carrasco, B. (2000). Calculation of hydrodynamic properties of globular proteins from their atomic-level structure. Biophys. J. *78*, 719-730.

Gill, D. J., Teo, H., Sun, J., Perisic, O., Veprintsev, D. B., Emr, S. D., and Williams, R. L. (2007). Structural insight into the ESCRT-I/-II link and its role in MVB trafficking. Embo J *26*, 600-612.

Hierro, A., Kim, J., and Hurley, J. H. (2005). Polycistronic expression and purification of the ESCRT-II endosomal trafficking complex. Methods Enzymol *403*, 322-332.

Hoover, D. M., and Lubkowski, J. (2002). DNA Works: an automated method for designing oligonucleotides for PCR-based gene synthesis. Nucleic Acids Res *30*, e43.

Janke, C., Magiera, M. M., Rathfelder, N., Taxis, C., Reber, S., Maekawa, H., Moreno-Borchart, A., Doenges, G., Schwob, E., Schiebel, E., and Knop, M. (2004). A versatile toolbox for PCR-based tagging of yeast genes: new fluorescent proteins, more markers and promoter substitution cassettes. Yeast *21*, 947-962.

Jones, T. A., Zou, J. Y., Cowan, S. W., and Kjeldgaard, M. (1991). Improved Methods for Building Protein Models in Electron- Density Maps and the Location of Errors in These Models. Acta Crystallogr. Sect. A *47*, 110-119.

Lebowitz, J., Lewis, M. S., and Schuck, P. (2002). Modern analytical ultracentrifugation in protein science: A tutorial review. Protein Sci. *11*, 2067-2079.

Longtine, M. S., McKenzie, A., Demarini, D. J., Shah, N. G., Wach, A., Brachat, A., Philippsen, P., and Pringle, J. R. (1998). Additional modules for versatile and economical PCR-based gene deletion and modification in Saccharomyces cerevisiae. Yeast *14*, 953-961.

Pineda-Molina, E., Belrhali, H., Piefer, A. J., Akula, I., Bates, P., and Weissenhorn, W. (2006). The crystal structure of the C-terminal domain of Vps28 reveals a conserved surface required for Vps20 recruitment. Traffic *7*, 1007-1016.
Piper, R. C., Cooper, A. A., Yang, H., and Stevens, T. H. (1995). Vps27 Controls Vacuolar And Endocytic Traffic Through A Prevacuolar Compartment In Saccharomyces-Cerevisiae. J. Cell Biol. *131*, 603-617.
Reggiori, F., and Pelham, H. R. B. (2001). Sorting of proteins into multivesicular bodies: ubiquitin-dependent and -independent targeting. Embo J. *20*, 5176-5186.
Rost, B., and Liu, J. F. (2003). The PredictProtein server. Nucleic Acids Res. *31*, 3300-3304.
Schuck, P. (2003). On the analysis of protein self-association by sedimentation velocity analytical ultracentrifugation. Analytical Biochemistry *320*, 104-124.
Sheff, M. A., and Thorn, K. S. (2004). Optimized cassettes for fluorescent protein tagging in Saccharomyces cerevisiae. Yeast *21*, 661-670.
Sheffield, P., Garrard, S., and Derewenda, Z. (1999). Overcoming expression and purification problems of RhoGDI using a family of "parallel" expression vectors. Protein Expr. Purif. *15*, 34-39.
Tan, S. (2001). A Modular Polycistronic Expression System for Overexpressing Protein Complexes in Escherichia coli. Protein Expr. Purif. *21*, 224-234.
Teo, H., Veprintsev, D. B., and Williams, R. L. (2004). Structural insights into endosomal sorting complex required for transport (ESCRT-I) recognition of ubiquitinated proteins. J. Biol. Chem. *279*, 28689-28696.
Teo, H. L., Gill, D. J., Sun, J., Perisic, O., Veprintsev, D. B., Vallis, Y., Emr, S. D., and Williams, R. L. (2006). ESCRT-I core and ESCRT-II GLUE domain structures reveal role for GLUE in linking to ESCRT-I and membranes. Cell *125*, 99-111.
Terwilliger, T. C. (2000). Maximum-likelihood density modification. Acta Crystallogr. Sect. D-Biol. Crystallogr. *56*, 965-972.
Terwilliger, T. C., and Berendzen, J. (1999). Automated MAD and MIR structure solution. Acta Crystallogr. Sect. D-Biol. Crystallogr. *55*, 849-861.
Thompson, J. D., Gibson, T. J., Plewniak, F., Jeanmougin, F., and Higgins, D. G. (1997). The CLUSTAL-X windows interface: flexible strategies for multiple sequence alignment aided by quality analysis tools. Nucleic Acids Res *25*, 4876-4882.
Tong, A. H. Y., Evangelista, M., Parsons, A. B., Xu, H., Bader, G. D., Page, N., Robinson, M., Raghibizadeh, S., Hogue, C. W. V., Bussey, H.*, et al.* (2001). Systematic genetic analysis with ordered arrays of yeast deletion mutants. Science *294*, 2364-2368.
Urbanowski, J. L., and Piper, R. C. (2001). Ubiquitin Sorts Proteins into the Intralumenal Degradative Compartment of the Late-Endosome/Vacuole. Traffic *2*, 622-630.
Yamakawa, H. (1971). Modern Theory of Polymer Solutions (New York: Harper & Row).

Table S1

Statistics of Data Collection, MAD+MIR Phasing, and Crystallographic Refinement

Crystal	Native	SeMet		$AuCl_3$ Der. #1	$AuCl_3$ Der. #2	K_2PtCl_4
Heavy atom soaking condition				1 mM, 15 min	1 mM, 30 min	1 mM, 30 min
X-ray source	SER-CAT 22-ID	SER-CAT 22-ID		SER-CAT 22-BM	SER-CAT 22-BM	SER-CAT 22-BM
Wavelength (Å)	0.9795	0.9794	0.9717	1.0332	1.0332	1.0688
Space Group	I222	I222		I222	I222	I222
Unit Cell (Å)	a = 68.1	a = 68.3		a = 68.0	a = 68.2	a = 68.3
	b = 83.8	b = 83.7		b = 83.7	b = 83.7	b = 83.3
	c = 269.1	c = 267.7		c = 269.2	c = 268.5	c = 268.5
	$\alpha=\beta=\gamma=90^o$	$\alpha=\beta=\gamma=90^o$		$\alpha=\beta=\gamma=90^o$	$\alpha=\beta=\gamma=90^o$	$\alpha=\beta=\gamma=90^o$
Resolution (Å) [a]	2.7 [2.80-2.70]	3.75[3.88-3.75]	3.6 [3.73-3.60]	3.2 [3.31-3.20]	3.0 [3.11-3.00]	3.0 [3.11-3.00]
No. of unique reflections	19506	8049	8785	12267	13901	14584
I/σ [a]	29.7 [2.75]	19.4 [2.14]	19.6 [2.87]	17.3 [2.82]	18.1 [3.40]	26.9 [4.67]
R_{sym} (%) [a,b]	5.7 [38.5]	9.2 [45.9]	8.9 [40.1]	10.0 [39.6]	8.6 [35.3]	6.6 [31.2]
Data completeness (%)	90.8 [61.5]	97.5 [95.3]	97.8 [87.5]	93.3 [71.0]	87.0 [48.9]	93.7 [68.6]
Phasing and refinement statistics						
Mean FOM (20 - 3.0 Å) [c]				0.54 (SOLVE)		
Overall FOM (20 – 3.0 Å) [c]				0.58 (RESOLVE)		
$R_{working}$ (%) [a,d]	23.5					
R_{free} [c] (%) [a,e]	31.8					
R.m.s. bond length (Å)	0.008					
R.m.s. bond angle (°)	1.2					
Residues in most favored ϕ,ψ region (%)	88.0					

[a] The values in brackets relate to highest resolution shells.

[b] $R_{sym} = \Sigma_h\Sigma_i|I_i(h) - < I(h) >|/\Sigma_h\Sigma_i I_i(h)$.

[c] Resulting data from combining MAD and MIR phasing data in SOLVE/RESOLVE

[d] $R_{working} = \Sigma\ (|F_{obs}| - k|F_{calc}|) / \Sigma|F_{obs}|$.

[e] R_{free} is the R value calculated for 5% of the data randomly selected and withheld from structural refinement.

Table S2
Hydrodynamic Properties of the ESCRT-I Complex and its Variants

Complex	Mass of 1:1:1:1 complex / Da	Experimental mass / kDa	Experimental $s_{20,w}$ / 10^{-13} s	Calculated $s_{20,w}$ / 10^{-13} s	f/f_o	R_H (nm)
Tetramer core	65,775.2	--	3.25 ± 0.05	3.20	1.78 ± 0.03	4.76 ± 0.08
Tetramer ΔUEV	86,521.1	86.9 ± 3.0	3.80 ± 0.01	--	1.83 ± 0.01	5.36 ± 0.02
Intact Tetramer	108,046.7	117 ± 4.6	4.15 ± 0.05	--	1.93 ± 0.03	6.10 ± 0.08
Trimer ΔUEV	78,057.3	--	3.6 ± 0.1	--	1.75 ± 0.05	4.97 ± 0.14

Equilibrium sedimentation data for the trimer ΔUEV (Vps23 Δ1-161) construct were previously reported by Kostelansky et al. (2006).

Table S3.
CPY secretion, Mvb12 localization and Sna3 sorting phenotypes of Vps23, Mvb12 and Vps37 stalk mutants.

Mutant	CPY missorting[a]	Mvb12-GFP localization in *vps4*Δ[b]	Sna3 sorting
Vps23^{WT}	-	++++	++
*vps23*Δ	++++	-	-
Vps23^{M254D}	++	+	+/-
Vps23^{L286D}	++++	+	-
Vps23$^{M254D/L286D}$	++++	+/-	-
Vps23$^{F261D/L286D}$	++++	+/-	n.d.
Vps23$^{I265D/L286D}$	++++	+/-	n.d.
Vps23$^{V275D/L286D}$	++++	+/-	n.d.
Vps23$^{I279D/L286D}$	++++	+/-	n.d.
Vps23$^{L286D/I290D}$	++++	+/-	n.d.
Mvb12^{WT}	-	++++	++
*mvb12*Δ	++	-	+
Mvb12$^{C54D/I57D}$	+/-	+/-	+
Mvb12$^{L47D/I57D}$	+/-	+/-	+
Mvb12$^{L47D/H64D}$	+	+/-	+
Mvb12$^{L47D/I57D/H64D}$	+	n.d.	n.d.
Mvb12$^{L14D//L47D/H64D}$	++	n.d.	n.d.

$Mvb12^{K82stop}$	+	n.d.	n.d.
$Vps37^{WT}$	-	++++	++
*vps37*Δ	++++	-	-
$Vps37^{F88D}$	-	++++	++
$Vps37^{F99D}$	-	++++	n.d.
$Vps37^{F106D}$	-	++++	n.d.
$Vps37^{I92D}$	-	++++	++
$Vps37^{L102D}$	-	++++	n.d.
$Vps37^{F88D/I92D}$	-	++++	++
$Vps37^{F95D/F99D}$	+++	++	-
$Vps37^{I92D/L102D}$	+++	++	-
$Vps37^{F88D/F99D}$	++	++	+
$Vps37^{L67D}$	++	++	+
$Vps37^{L75D}$	++	++	n.d.
$Vps37^{V79D}$	++	++	+
$Vps37^{\Delta 1-21}$	-	++++	++

[a]CPY secretion of each mutant was quantitated by densitometry of CPY overlay assay and compared to the secretion of the corresponding null mutant. Note that *mvb12*Δ mutants secrete approximately 10% as much CPY as *vps23*Δ or *vps37*Δ mutants in this assay.

[b]Localization of Mvb12-GFP the MVB as determined by the brightness of punctate structures. Note lower steady-state levels of Mvb12-GFP in some mutants result in lower apparent intensity at the MVB.

Table S4. Yeast strains used in this study.

Strain	Genotype	Source
BY4742	MATα *his3Δ1 leu2Δ0 lys2Δ0 ura3Δ0*	Open Biosystems
BY4741	MAT**a** *his3Δ1 leu2Δ0 met15Δ0 ura3Δ0*	Open Biosystems
BY4742-14836	BY4742 *mvb12Δ::KanR*	Open Biosystems
BY4742-15588	BY4742 *vps4Δ::KanR*	Open Biosystems
BY4742-15381	BY4742 *vps27Δ::KanR*	Open Biosystems
BY4742-13416	BY4742 *vps23Δ::KanR*	Open Biosystems
BY4742-12730	BY4742 *vps37Δ::KanR*	Open Biosystems
BY4742-12763	BY4742 *vps28Δ::KanR*	Open Biosystems
BY4742-12826	BY4742 *vps22Δ::KanR*	Open Biosystems
BY4742-16211	BY4742 *vps20Δ::KanR*	Open Biosystems
SHY 8	BY4742 *MVB12::GFP-HIS3*	This study
SHY13	BY4742 *vps27Δ::KanR MVB12::GFP-HIS3*	This study
SHY10	BY4742 *vps28Δ::KanR MVB12::GFP-HIS3*	This study
SHY11	BY4742 *vps22Δ::KanR MVB12::GFP-HIS3*	This study
SHY9	BY4742 *vps4Δ::KanR MVB12::GFP-HIS3*	This study
CSY49	BY4742 *vps23Δ::KanR MVB12::GFP-HIS3*	This study
CSY50	BY4742 *vps37Δ::KanR MVB12::GFP-HIS3*	This study
CSY48	BY4742 *vps20Δ::KanR MVB12::GFP-HIS3*	This study
CTY365	BY4742 *vps36Δ::KanR MVB12::GFP-HIS3*	This study
SHY34	BY4742 *vps27Δ::KanR MVB12::GFP-HIS3 vps4Δ::NatR*	This study
CSY41	BY4742 *vps23Δ::KanR MVB12::GFP-HIS3 vps4Δ::NatR*	This study
CSY42	BY4742 *VPS23::6HA-NatR*	This study
CSY52	BY4742 *MVB12::GFP-HIS3 VPS23::6HA-NatR*	This study
CSY46	BY4742 *vps27Δ::KanR MVB12::GFP-HIS3*	This study

	VPS23::6HA-NatR	
CSY47	BY4742 *vps4*Δ::*KanR MVB12::GFP-HIS3 VPS23::6HA-NatR*	This study
CSY45	BY4742 *vps28*Δ::*KanR MVB12::GFP-HIS3 VPS23::6HA-NatR*	This study
CSY53	BY4742 *vps37*Δ::*KanR MVB12::GFP- HIS3 VPS23::6HA-NatR*	This study
CSY63	BY4742 *mvb12*Δ::*KanR vps4*Δ*::NatR*	This study
CSY64	BY4742 *mvb12*Δ::*KanR VPS23::6HA-NatR*	This study
CSY65	BY4742 *vps23*Δ::*KanR VPS37::13myc-HIS3*	This study
CSY67	BY4742 *mvb12*Δ::*KanR VPS37::13myc-HIS3*	This study
CSY62	BY4742 *vps37*Δ::*KanR VPS23::6HA-NatR*	This study
CTY364	BY4742 *vps37*Δ::*KanR vps4*Δ*::NatR MVB12::GFP-HIS3*	This study
CTY362	BY4742 *mvb12*Δ::*KanR VPS23::GFP- HIS3*	This study
CTY363	BY4742 *mvb12*Δ::*KanR vps4*Δ*::NatR VPS23::GFP- HIS3*	This study
CTY361	BY4742 *vps37*Δ::*KanR VPS23::GFP- HIS3*	This study

Figure S1

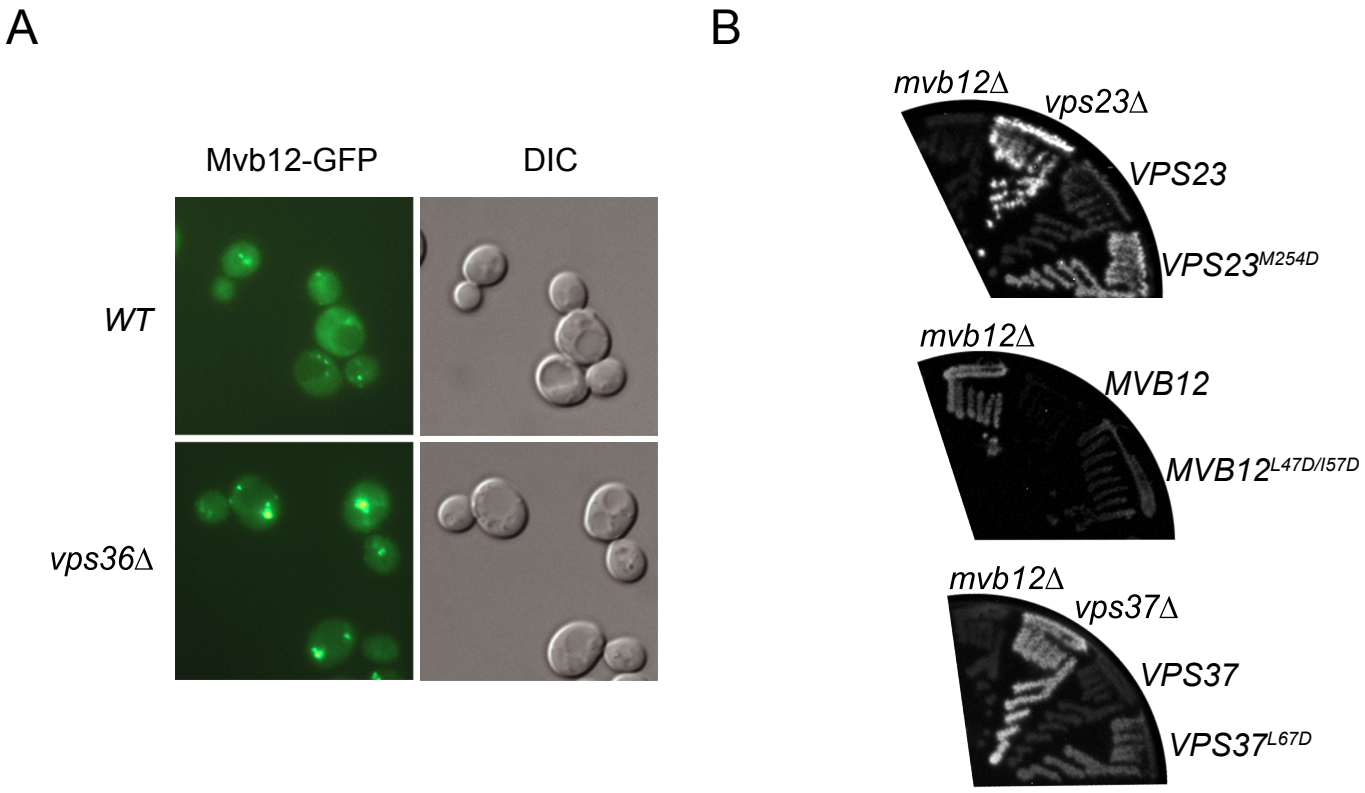
A
Mvb12-GFP
DIC
WT
vps36Δ
B
mvb12Δ
vps23Δ
VPS23
VPS23M254D
mvb12Δ
MVB12
MVB12L47D/I57D
mvb12Δ
vps37Δ
VPS37
VPS37L67D
C
VPS37-13myc
MVB12-GFP
VPS37-13myc
VPS23-6HA
MVB12-GFP/ VPS23-6HA
pVPS23
pRS416
pVPS23M254D
pVPS23
pRS416
pVPS23M254D
pMVB12
pRS416
pMVB12L47S/I57D
pMVB12
pRS416
pMVB12L47S/I57D
pVPS37
pRS416
pVPS37L67D
α-myc
α-HA
α-GFP
α-Dpm1

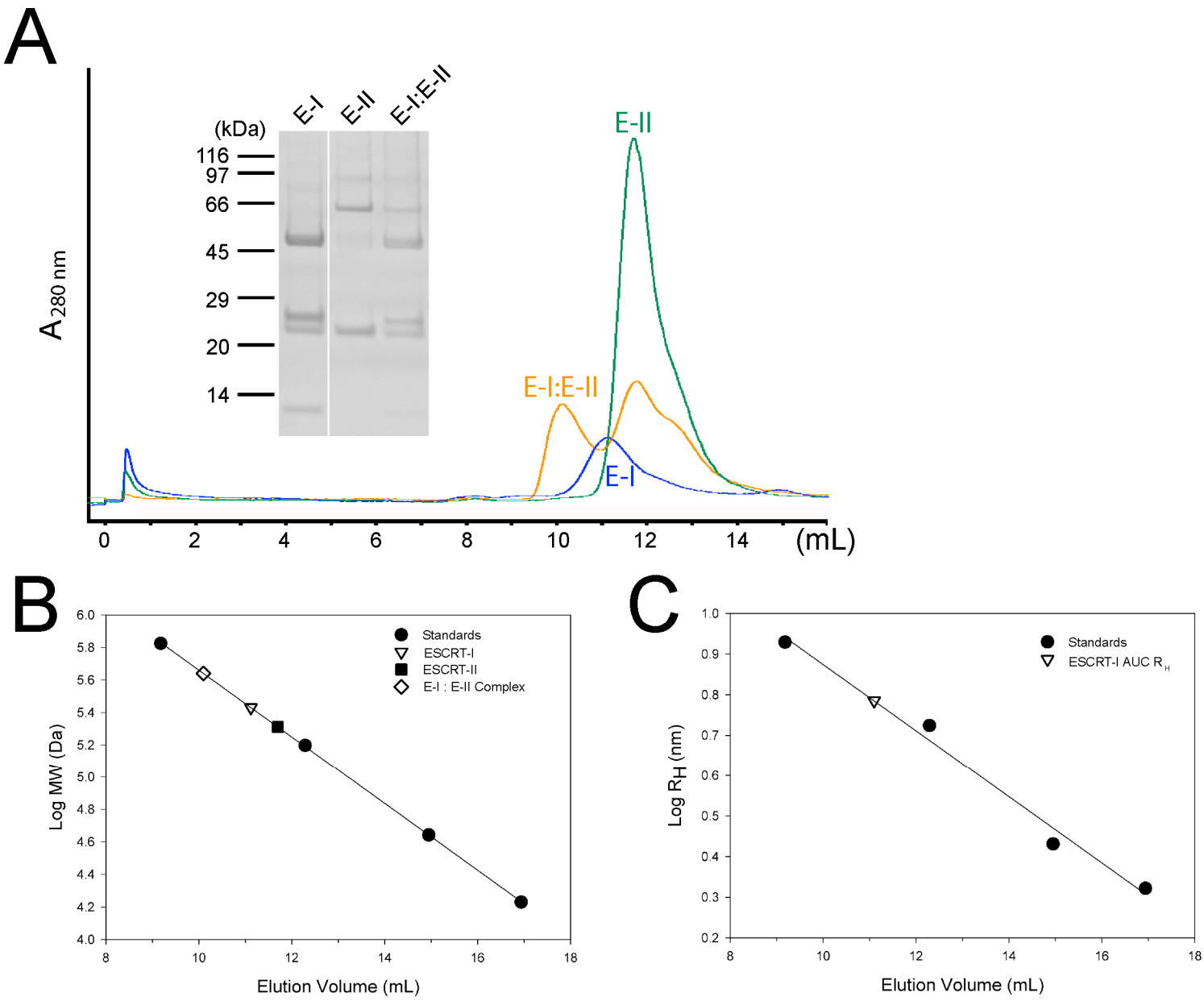
A
A280 nm
(kDa)
116
97
66
45
29
20
14
E-I
E-II
E-I:E-II
E-II
E-I:E-II
E-I
0
2
4
6
8
10
12
14
(mL)
B
Log MW (Da)
Standards
ESCRT-I
ESCRT-II
E-I : E-II Complex
Elution Volume (mL)
C
Log RH (nm)
Standards
ESCRT-I AUC RH
Elution Volume (mL)

Figure S2

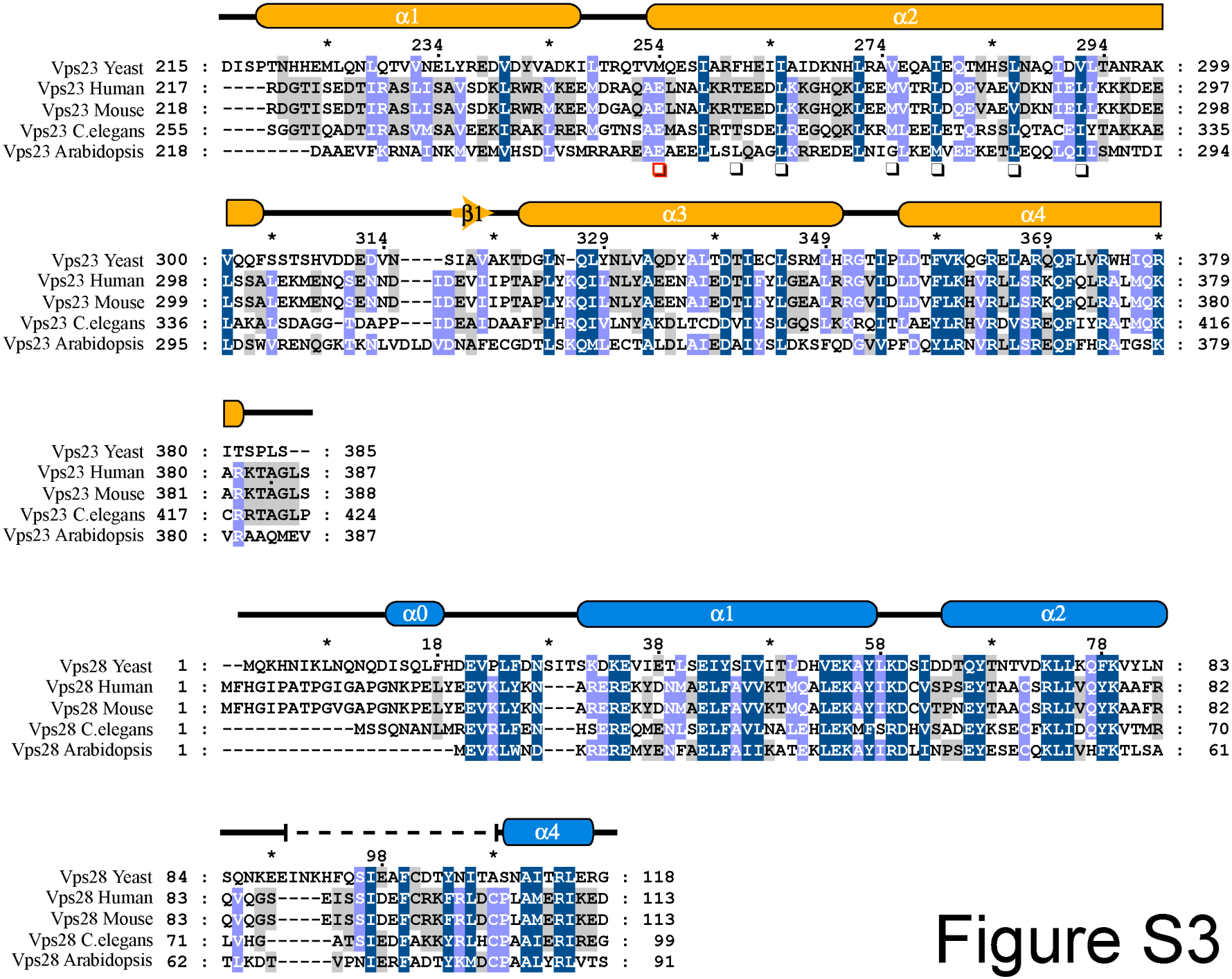
α1
α2
β1
α3
α4
α0
Vps23 Yeast
Vps23 Human
Vps23 Mouse
Vps23 C.elegans
Vps23 Arabidopsis
Vps28 Yeast
Vps28 Human
Vps28 Mouse
Vps28 C.elegans
Vps28 Arabidopsis

Figure S3

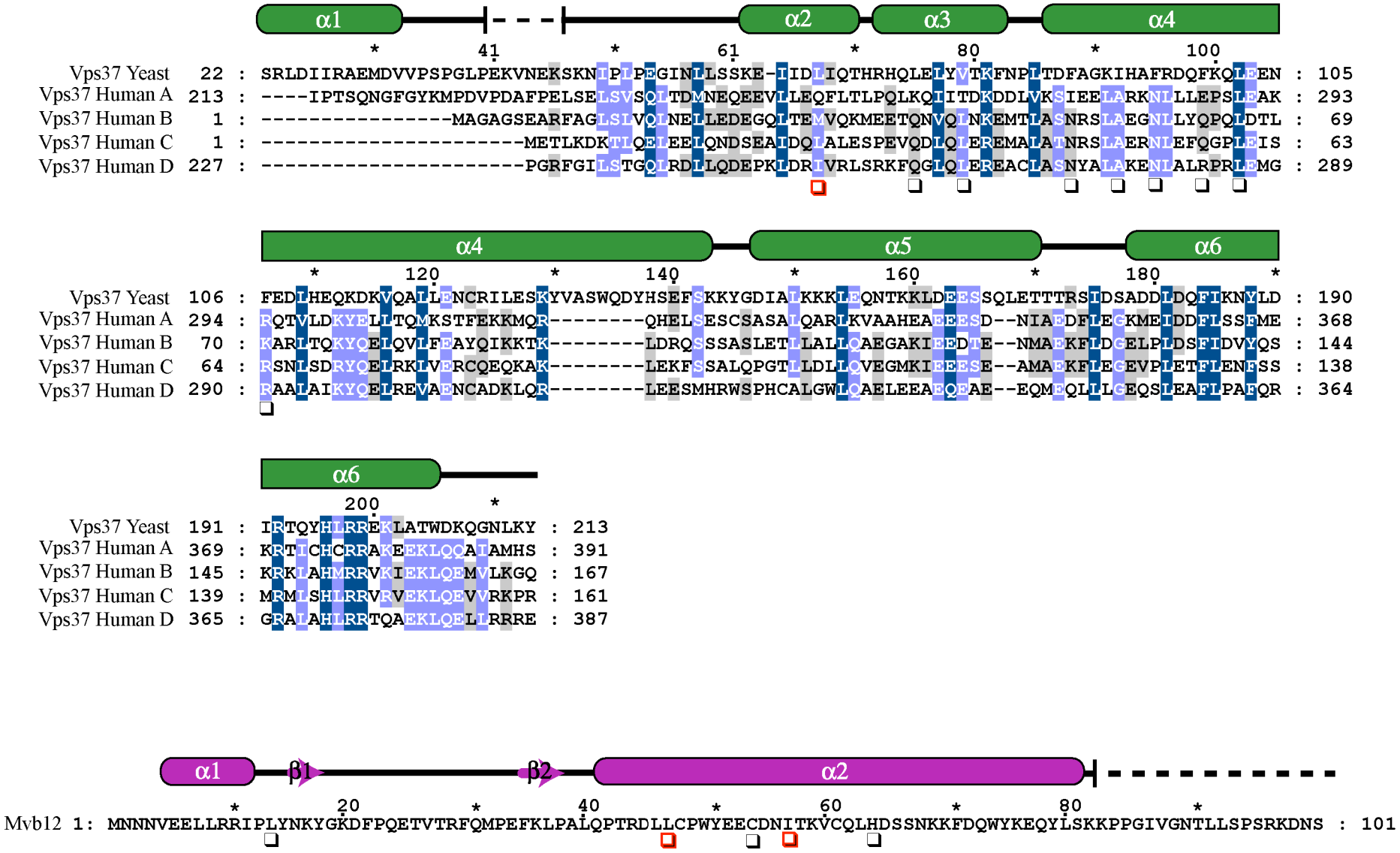
α1
α2
α3
α4
α5
α6
β1
β2
Vps37 Yeast
Vps37 Human A
Vps37 Human B
Vps37 Human C
Vps37 Human D
Myb12

Figure S4

Figure S5

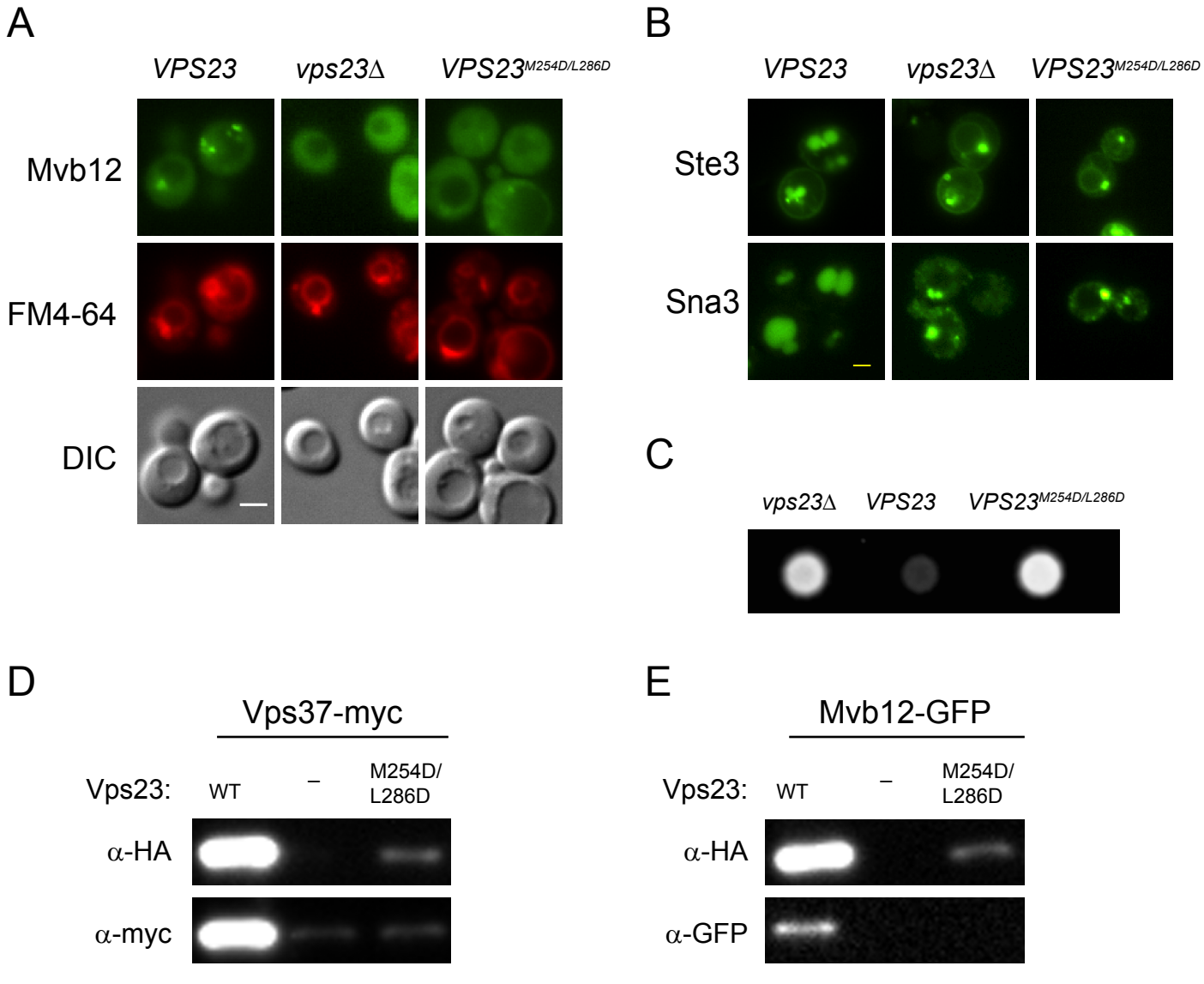
A
VPS23
vps23Δ
VPS23M254D/L286D
Mvb12
FM4-64
DIC
B
VPS23
vps23Δ
VPS23M254D/L286D
Ste3
Sna3
C
vps23Δ
VPS23
VPS23M254D/L286D
D
Vps37-myc
Vps23:
WT
–
M254D/
L286D
α-HA
α-myc
E
Mvb12-GFP
Vps23:
WT
–
M254D/
L286D
α-HA
α-GFP